Structural and Electrochemical Properties of Iridium–Carbon Bonded Metalloporphyrins. Characterization of (OEP)Ir(C_8H_{13}) and (OEP)Ir(C_8H_{13})(CO)

J.-L. Cornillon, J. E. Anderson, C. Swistak, and K. M. Kadish*

Contribution from the Department of Chemistry, University of Houston, Houston, Texas 77004. *Received April 28, 1986*

Abstract: An electrochemical and structural study of (OEP)Ir(C_8H_{13}), where OEP is the dianion of octaethylporphyrin and C_8H_{13} is the *cis*-bicyclo(3.3.0)oct-1-yl group, is reported. (OEP)Ir(C_8H_{13}) was found to crystallize in the $P\bar{1}$ space group with a = 12.78 Å, b = 13.33 Å, c = 14.20 Å, α = 58.75°, β = 69.57°, γ = 67.15 Å, and z = 2. The Ir atom is displaced only 0.08 Å from the porphyrin plane, and the iridinium–carbon bond distance was found to be 1.89 Å. This is the first reported crystal structure of an iridium porphyrin complex as well as the first example where a bicyclic ligand is σ bonded to a metalloporphyrin. Two-dimensional NMR techniques were also performed and demonstrate that the structure of (OEP)Ir(C_8H_{13}) is basically the same in solution as in the solid state. The five coordinate complex reversibly binds with CO to form (OEP)Ir(C_8H_{13})(CO), and a formation constant of K_{eq} = 340 ± 200 atm^{-1} was measured for this ligand binding reaction. In addition, detailed electrochemistry and spectroelectrochemistry of (OEP)Ir(C_8H_{13}) and (OEP)Ir(C_8H_{13})(CO) are reported in nonaqueous media, and a complete electrochemical mechanism for oxidation and reduction of both species is presented. Of particular interest is the fact that (OEP)Ir(C_8H_{13}) provides the first example of a σ-bonded metalloporphyrin which can be reversibly oxidized at the σ-bonded axial ligand without a cleavage of the metal–carbon bond.

The synthesis of iridium porphyrins has been known for some time,[1,2] but only a few reports have been published on the chemistry and characterization of these complexes.[3–5] A detailed electrochemical study of alkyliridium porphyrin complexes has never been reported nor has any structural data ever been published on iridium porphyrin complexes. This is surprising given the large body of knowledge on the catalytic and organometallic nature of different nonporphyrin iridium compounds[6,7] and the current interest in related rhodium porphyrins.[8–12]

In this paper we present a molecular structure determination of (OEP)Ir(C_8H_{13}) both in the solid state and in solution with an aim of examining the stability of this iridium carbon bonded species. This compound is isolated from the metalation reaction of $(OEP)H_2$ with $[Ir(COD)Cl]_2$, where COD = 1,5 cyclooctadiene.[2] The structure of (OEP)Ir(C_8H_{13}) represents the first reported crystal structure of an iridium porphyrin complex as well as the first example where a bicyclic ligand is σ bonded to a metalloporphyrin. Two dimensional NMR techniques were also performed and correlations made between the structure of (OEP)Ir(C_8H_{13}) in solution and in the solid state.

The electrochemistry of three transition metal and two Group 13 σ-bonded metalloporphyrins has been reported to date.[13–17] In most cases the electrooxidation is irreversible and involves one of two types of chemical reactions following electron abstraction. The first oxidation of (P)M(R), where the central metal M is Rh,[14] In,[15] or Ga[16] and R is an alkyl(aryl) group, results in metal–carbon bond cleavage and formation of (P)M(X), where X is the anion of the supporting electrolyte. The first oxidation of (TPP)Fe(C_6H_5) and (OEP)Fe(C_6H_5)[13] results in a reversible migration of the phenyl group from the Fe atom to one of the pyrrole nitrogens. This electrooxidation proceeds via an ECE mechanism. Migration after electrooxidation also occurs for σ-bonded alkyl (aryl) cobalt porphyrins.[17] The electrochemistry of (OEP)Ir(C_8H_{13}) is different than any previously investigated σ-bonded metalloporphyrin but has some characteristics similar to those of the cobalt σ-bonded complexes.

A CO adduct of (OEP)Ir(C_8H_{13}) is also formed. The electrochemistry and spectroelectrochemistry of (OEP)Ir(C_8H_{13}) and (OEP)Ir(C_8H_{13})(CO) are reported in nonaqueous media, and a complete electrochemical mechanism for oxidation and reduction of both species is presented. The presence of bound CO stabilizes the one-electron reduction product but destabilizes the one-electron oxidation product. These reactions are discussed in detail.

Experimental Section

Materials. Dichloroethane (DCE) was purchased from Aldrich (HPLC grade) and purified by double distillation from CaH_2. Tetrahydrofuran (THF) was purchased from Aldrich (HPLC grade) and purified by distillation from Na/benzophenone. Deuterated benzene-d_6 (Aldrich) was distilled from Na/benzophenone. All solvents were distilled under inert atmosphere prior to use. Tetrabutylammonium perchlorate ($TBA(ClO)_4$) was purchased from Aldrich, recrystallized twice from absolute ethanol, dried, and stored under vacuum at 45 °C. High purity nitrogen and carbon monoxide and a 10% carbon monoxide–argon mixture were purchased from IWECO and Matheson, respectively.

(OEP)Ir(C_8H_{13}) was synthesized by literature methods.[2] Single crystals of (OEP)Ir(C_8H_{13}) suitable for X-ray diffraction were grown by the slow diffusion of pentane vapor into a concentrated benzene solution of (OEP)Ir(C_8H_{13}) at a constant temperature (24 °C).

Instrumentation. Cyclic voltammetry measurements were performed with the use of a conventional three electrode system. The working electrode was a gold button (A = 0.85 mm^2). A commercial saturated calomel electrode was typically used as the reference electrode, but in some cases a silver wire pseudo-reference electrode was used. The ref-

(1) Sadasivan, N.; Fleischer, E. B. *J. Inorg. Nucl. Chem.* **1968**, *30*, 591.
(2) Ogoshi, H.; Setsune, J.; Yoshida. Z. *J. Organomet. Chem.* **1978**, *159*, 317.
(3) Sugimoto, H.; Ueda, N.; Mori, M. *J. Chem. Soc., Dalton Trans.* **1982**, 1611.
(4) Pierce, R. M. Dissertation Thesis, University of Pennsylvania, 1983.
(5) Antipas, A.; Gouterman, M. *J. Am. Chem. Soc.* **1983**, *105*, 4896.
(6) Leigh, G. J.; Richards, R. L. In *Comprehensive Organometallic Chemistry*; Wilkinson, G., Ed.; Pergamon Press: New York, 1982; Vol. 5, p 541.
(7) Cotton, F. A.; Wilkinson, G. *Advanced Inorganic Chemistry*, 4th ed.; Wiley: New York, 1980; p 934.
(8) Aoyama, Y.; Fujisawa, T.; Wantanabe, T.; Toi, H.; Ogoshi, H. *J. Am. Chem. Soc.* **1986**, *108*, 943.
(9) Aoyama, Y.; Yoshida, T.; Sakurai, K.; Ogoshi, H. *Organometallics* **1986**, *5*, 168.
(10) Jones, N. L.; Carroll, P. J.; Wayland, B. B. *Organometallics* **1986**, *5*, 313.
(11) Wayland, B. B.; Del Rossi, K. J. *J. Am. Chem. Soc.* **1985**, *107*, 7941.
(12) Kadish, K. M.; Yao, C.-L.; Anderson, J. E.; Cocolios, P. *Inorg. Chem.* **1985**, *24*, 4515.
(13) Lançon, D.; Cocolios, P.; Guilard, R.; Kadish, K. M. *J. Am. Chem. Soc.* **1984**, *106*, 4472.
(14) Kadish, K. M.; Anderson, J. E.; Yao, C.-L.; Guilard, R. *Inorg. Chem.* **1986**, *25*, 1277.
(15) Kadish, K. M.; Boisselier-Cocolios, B.; Cocolios, P.; Guilard, R. *Inorg. Chem.* **1985**, *24*, 2139.
(16) Kadish, K. M.; Boisselier-Cocolios, B.; Coutsolelos, A.; Mitaine, P.; Guilard, R. *Inorg. Chem.* **1985**, *24*, 4521.
(17) (a) Callot, H. J.; Metz, F. *J. Chem. Soc., Chem. Commun.* **1982**, 947. (b) Callot, H. J.; Cromer, R *Nouv. J. Chim.* **1984**, *8*, 765 and references therein.

0002-7863/86/1508-7633$01.50/0

Table I. Data Collection and Processing Parameters for (OEP)Ir(C_8H_{13})

space group	$P\bar{1}$, triclinic
cell constants	a = 12.789 (3) Å
	b = 13.327 (6) Å
	c = 14.200 (5) Å
	α = 58.73 (5)°
	β = 69.57 (2)°
	γ = 67.15 (4)°
unit cell volume	187 Å^3
molecular formula	$IrC_{44}H_{57}N_4$
formula wt	834.2
formula units per cell	Z = 2
density (calcd)	ρ = 1.48 g/cm^{-3}
absorption coeff	μ = 35.8 cm^{-1}
radiation (Mo Kα)	λ = 0.71073 Å
collectn range	4° ≤ 2θ ≤ 35°
scan width	$\Delta\theta$ = (1.10 + 0.35 tan θ)°
max scan time	120 s
scan speed range	0.9–5.0 deg min^{-1}
total data collected	2369
independent data, $I > 3\sigma(I)$	2111
total variables	402
$R = \Sigma\|\|F_o\| - \|F_c\|\|/\Sigma\|F_o\|$	0.052
$R_w = [\Sigma w(\|F_o\| - \|F_c\|)^2/\Sigma w\|F_o\|^2]^{1/2}$	0.060

erence electrode, in either case, was separated from the bulk solution by a fritted glass bridge which contained the nonaqueous solvent and supporting electrolyte. Potentials were referenced to the ferrocene/ferrocenium (Fc/Fc^+) couple when the silver wire pseudo-reference electrode was used. An EG&G Model 173 potentiostat, an EG&G Model 175 Universal programmer, and a Houston Instrument Model 2000 X-Y recorder, or a BAS 100 electrochemical analyzer was used for cyclic voltammetry experiments. Controlled potential electrolysis was performed with an EG&G Model 173 potentiostat or a BAS 100. Rotating disk electrode experiments (RDE) were performed by using an IBM EC 1219 rotating disk electrode controller coupled with one of the above listed electrochemical instruments. Both the reference electrode and the platinum grid counter electrode were separated from the bulk solution by means of a fritted glass bridge.

Unless otherwise noted, 0.1 M supporting electrolyte was used for electrochemical experiments, while the sample concentration ranged from 0.5×10^{-4} to 1×10^{-3} M. Thin-layer spectroelectrochemical measurements were performed with an IBM EC 225 voltammetric analyzer coupled with a Tracor Northern 1710 holographic optical spectrometer multichannel analyzer to obtain spectral data either as a function of potential or time. The construction and properties of the optically transparent thin-layer electrode have been described in the literature.[18]

Titrations of (OEP)Ir(C_8H_{13}) with carbon monoxide were performed by using a Matheson Model 8250 modular dyna-blender and flow meters. The gas flow meters allowed for argon–carbon monoxide mixtures of known concentration to be passed through the solution of porphyrin. Partial pressures of CO between 0.005 and 1 atmosphere were reached by using either pure CO or the commercially obtained 10% CO/Ar mixture as the source of carbon monoxide. Correction for the vapor pressures of THF or DCE were made where applicable.

NMR spectra were obtained on a Nicolet NT-300 spectrometer controlled by a Model 293-C pulse programmer and equipped with a 5-nm $^1H/^{13}C$ dual tuned probe. The sample used for the COSY and heteronuclear $^1H/^{13}C$ chemical shift correlation was prepared by dissolving 30 mg of (OEP)Ir(C_8H_{13}) in 0.5 mL of deuterated benzene. All spectra were recorded at 30 °C. Pulse sequences for the COSY and heteronuclear $^1H/^{13}C$ chemical shift correlation have been described elsewhere.[19] An IBM Model ED-100 electron spin resonance system was used to record ESR spectra. IR spectra were taken on an IBM Model 32 FTIR spectrophotometer.

Crystal Structure Determination. Single crystal X-ray analysis of (OEP)Ir(C_8H_{13}) was performed at the University of Houston X-ray Crystallography Center. A jet black parallelepiped of approximate dimensions 0.60 × 0.35 × 0.20 mm was mounted on a glass fiber in a random orientation on an Enraf-Nonius CAD-4 automatic diffractometer. Mo Kα radiation, monochromatized by a dense graphite crystal assumed for all purposes to be 50% imperfect, was used. Final cell constants as well as other information pertinent to data collection and refinement are listed in Table I. The Laue symmetry was determined to be 1, and the space group was therefore either P1 or $P\bar{1}$ and eventually found to be $P\bar{1}$. Intensities were measured by using the θ–2θ scan technique, with the scan rate depending on the net count obtained in rapid prescans of each reflection. Two standard reflections were monitored periodically during the course of the data collection as a check of crystal stability and electronic reliability. The standard reflections did not vary significantly over this period. In reducing the data, Lorentz and polarization factors were applied as well as an empirical absorption correction based on azimuthal ψ scans of six reflections having χ near 90°.[20]

The location of the Ir atom was determined by the Patterson method. The remaining atoms were found in subsequent difference Fourier syntheses. The C_8H_{13} ligand was found to have high thermal motion, which may account for the low crystal quality, indicated by broad peak scans noted prior to data collection. The usual sequence of isotropic and anisotropic refinement was followed, after which all hydrogens were located at ideally calculated positions. Anisotropic refinement was performed on only the Ir and OEP ring atoms. Final convergence was reached, indicated by all shift/esd ratios less than 0.2; final values of R = 5.2% and R_w = 6.0% were obtained. No unusually high correlations were noted between any of the variables in the last cycle of least-squares refinement, and the final difference density map showed no peaks greater than 0.20 e/Å^3. All calculations were made by using Molecular Structure Corporation's TEXRAY 230 modifications of the SDP-PLUS series of programs.

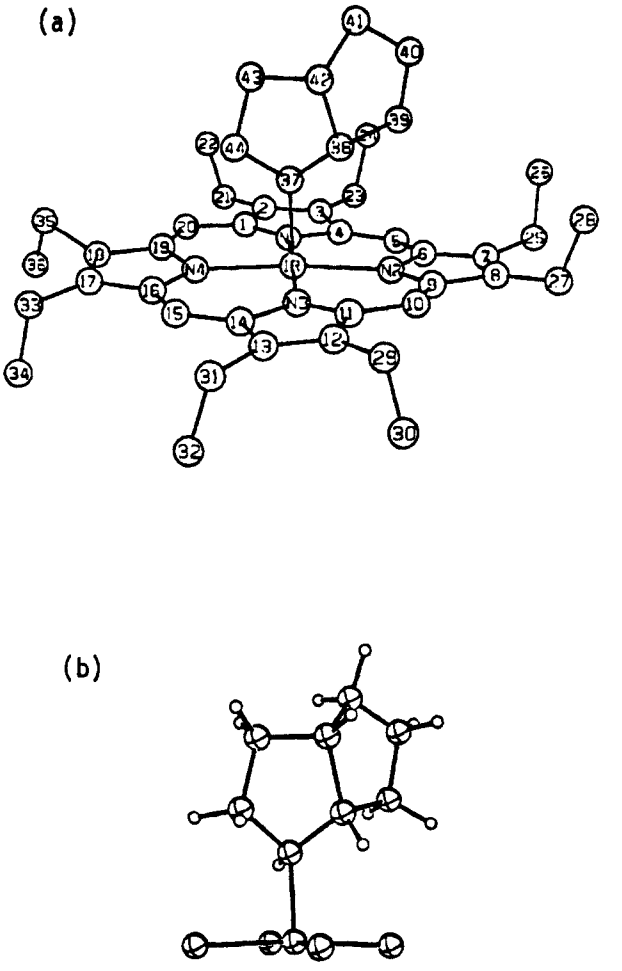

Figure 1. (a) Molecular structure of (OEP)Ir(C_8H_{13}) and numbering scheme and (b) central $N_4IrC_8H_{13}$ fragment of (OEP)Ir(C_8H_{13}).

Results and Discussion

The molecular structure of (OEP)Ir(C_8H_{13}), without the H atoms, is presented in Figure 1a, while a view of the central $N_4IrC_8H_{13}$ fragment is shown in Figure 1b. Table II gives the

(18) Lin, X.-Q.; Kadish, K. M. *Anal. Chem.* **1985**, *57*, 1498.

(19) (a) Aue, W. P.; Bartholdi, E.; Ernst, R. R. *J. Chem. Phys.* **1976**, *64*, 2229. (b) Martin, G. E. *J. Heterocycl. Chem.* **1978**, *15*, 1539. (c) Bax, A.; Freeman, R. *J. Magn. Reson.* **1981**, *44*, 542. (d) Reynolds, W. F.; Enriguez, R. G.; Escobar, L. I.; Lozoya, X. *Can. J. Chem.* **1984**, *62*, 2421. (e) Wynants, C.; Hallenga, K.; Van Binst, G.; Michel, A.; Zanen, J. *J. Magn. Reson.* **1984**, *57*, 93.

(20) North, A. C. T.; Phillips, D. C.; Matthews, F. S. *Acta Crystallogr., Sect. A: Cryst. Phys., Diffr. Theor. Gen. Crystallogr.* **1968**, *A24*, 351.

Table II. Positional Parameters and Their Estimated Standard Deviations

atom	*x*	*y*	*z*
Ir	0.11580 (6)	0.29670 (7)	0.03280 (6)
N1	0.001 (2)	0.389 (1)	−0.073 (1)
N2	−0.008 (1)	0.319 (1)	0.167 (1)
N3	0.232 (1)	0.216 (1)	0.132 (1)
N4	0.244 (1)	0.286 (1)	−0.104 (1)
C1	0.010 (2)	0.415 (2)	−0.177 (2)
C2	−0.096 (2)	0.478 (2)	−0.215 (1)
C3	−0.175 (1)	0.497 (2)	−0.131 (2)
C4	−0.121 (2)	0.449 (2)	−0.042 (2)
C5	−0.170 (2)	0.444 (2)	0.060 (2)
C6	−0.127 (2)	0.383 (2)	0.158 (2)
C7	−0.185 (2)	0.370 (2)	0.266 (2)
C8	−0.108 (2)	0.305 (2)	0.337 (1)
C9	0.008 (2)	0.273 (1)	0.271 (1)
C10	0.109 (1)	0.209 (2)	0.307 (1)
C11	0.217 (2)	0.182 (2)	0.240 (2)
C12	0.322 (2)	0.115 (2)	0.287 (1)
C13	0.407 (2)	0.114 (2)	0.119 (2)
C14	0.355 (2)	0.172 (2)	0.102 (2)
C15	0.406 (1)	0.184 (2)	−0.007 (2)
C16	0.362 (2)	0.235 (2)	−0.105 (2)
C17	0.421 (2)	0.237 (2)	−0.210 (1)
C18	0.337 (2)	0.286 (2)	−0.270 (2)
C19	0.225 (2)	0.317 (2)	−0.204 (1)
C20	0.119 (2)	0.374 (2)	−0.236 (1)
C21	−0.101 (2)	0.526 (2)	−0.334 (2)
C22	−0.121 (2)	0.448 (3)	−0.357 (2)
C23	−0.301 (1)	0.557 (2)	−0.136 (2)
C24	−0.365 (2)	0.468 (2)	−0.104 (2)
C25	−0.316 (2)	0.414 (2)	0.297 (2)
C26	−0.379 (2)	0.335 (2)	0.308 (2)
C27	−0.128 (2)	0.262 (2)	0.459 (1)
C28	−0.160 (2)	0.145 (2)	0.527 (2)
C29	0.339 (2)	0.061 (2)	0.404 (1)
C30	0.371 (2)	0.136 (2)	0.427 (2)
C31	0.538 (1)	0.063 (2)	0.192 (1)
C32	0.596 (2)	0.162 (2)	0.143 (2)
C33	0.549 (2)	0.199 (2)	−0.242 (1)
C34	0.602 (2)	0.293 (2)	−0.273 (2)
C35	0.348 (2)	0.284 (2)	−0.389 (3)
C36	0.361 (2)	0.390 (2)	−0.453 (2)
C37	0.088 (2)	0.151 (2)	0.067 (2)
C38	0.040 (2)	0.074 (2)	0.174 (2)
C39	−0.092 (2)	0.092 (2)	0.221 (2)
C40	−0.116 (3)	−0.028 (3)	0.272 (3)
C41	−0.049 (3)	−0.096 (3)	0.222 (2)
C42	0.073 (3)	−0.072 (3)	0.202 (3)
C43	0.138 (2)	−0.066 (2)	0.095 (2)
C44	0.179 (2)	0.049 (2)	0.039 (2)

Table III. Table of Selected Bond Distances of (OEP)Ir(C_8H_{13}) in Angstroms

atom 1	atom 2	distance	atom 1	atom 2	distance
Ir	N_1	2.041 (8)	C_{38}	C_{39}	1.55 (1)
Ir	N_2	2.083 (6)	C_{38}	C_{42}	1.67 (2)
Ir	N_3	2.041 (7)	C_{39}	C_{40}	1.48 (2)
Ir	N_4	2.087 (6)	C_{40}	C_{41}	1.30 (2)
Ir	C_{37}	1.893 (8)	C_{41}	C_{42}	1.61 (2)
C_{37}	C_{38}	1.40 (1)	C_{42}	C_{43}	1.43 (1)
C_{37}	C_{44}	1.53 (1)	C_{43}	C_{44}	1.53 (1)

final atomic positional parameters in fractional coordinates while Tables III and IV give select bond distances and bond angles, respectively.

The coordination about the iridium atom can be described as square pyrimidal. The average Ir–N bond distance is 2.05 Å and is the same as reported Ir–N distances in other nonporphyrin complexes,[21,22] typically near 2.08 Å. The iridium atom is only

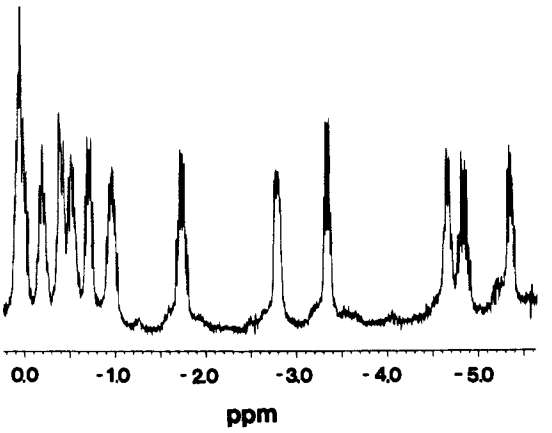

Figure 2. ^{1}H NMR spectrum of the signal arising from the C_8H_{13} group of (OEP)Ir(C_8H_{13}) in benzene-d_6.

0.08 Å out of the N_4 porphyrin plane. This is similar to (OEP)Rh(CH_3),[23] (OEP)Rh(CHO),[4] and (OEP)Rh(COC_6H_5)[24] where the rhodium atom is 0.051–0.075 Å out of the N_4 porphyrin plane. The small displacement of the iridium atom is surprising considering the size of the C_8H_{13} axial ligand and the size of the iridium atom. An interesting consequence of the location of the iridium atom is that the sixth coordination site is available for further ligand addition. As discussed later in this manuscript, CO readily binds to the (OEP)Ir(C_8H_{13}) complex.

Of particular interest is the Ir–C bond distance of 1.89 Å, which is below the reported range of 1.97–2.19 Å for Ir–C single bonds.[25,26] In addition, the distance of 1.89 Å is smaller than the 2.00-Å distance proposed[27] for a Ir–C double bond. The short Ir–C bond distance in (OEP)Ir(C_8H_{13}) reflects the strength of this bond and agrees well with the reaction chemistry and the electrochemistry of the compound.

The *cis*-bicyclo(3.3.0)oct-1-yl group (C_8H_{13}) did not refine especially well. This is demonstrated by the large thermal parameters[28] and the large range of carbon–carbon bond distances and bond angles observed for this fragment. Of interest is the long C(38) to C(42) bond distance of 1.67 Å. This suggests a fairly reactive site on the bicyclooctane ligand. However, the long bond may only be due to the variation of bond distances. All of the bond distances and angles for the octaethylporphyrin macrocycle are within expected ranges.[23,24,29,30]

NMR Spectral Studies. The ^{1}H NMR signals from the porphyrin ligand do not have any unusual variation from what has been reported.[31] They are characterized by resonances at 9.73, 3.94, and 1.88 ppm due to the meso, pyrrole-α-CH_2, and pyrrole-β-CH_3 protons, respectively. The ^{1}H NMR signal from the C_8H_{13} group is shown in Figure 2. The complexity of the signal reveals strong hydrogen coupling in this ligand. In addition, the strong upfield shift of the ^{1}H NMR signal for the C_8H_{13} ligand (between 0 and −6 ppm) indicates the influence of the porphyrin ring current. This is in general agreement with the crystal

(21) Rasmussen, P. G.; Bailey, O. H.; Bayon, J. C. *Inorg. Chem.* **1984**, *23*, 338.
(22) Rasmussen, P. G.; Anderson, J. E.; Bailey, O. H.; Tamres, M.; Bayon, J. C. *J. Am. Chem. Soc.* **1985**, *107*, 279.
(23) Takenaka, A.; Syal, S. K.; Sasada, Y.; Omura, T.; Ogoshi, H.; Yoshida, Z. *Acta Crystallogr., Sect. B: Struct. Crystallogr. Cryst. Chem.* **1976**, *32*, 62.
(24) Grigg, R. *Acta Crystallogr., Sect. B: Struct. Crystallogr. Cryst. Chem.* **1982**, *38*, 2455.
(25) Bezman, S. A.; Bird, P. N.; Fraser, A. R.; Osborn, J. A. *Inorg. Chem.* **1980**, *19*, 3755.
(26) Shultz, A. J.; McArdle, J. V.; Khamare, G. P.; Eisenberg, R. *J. Organomet. Chem.* **1974**, *72*, 415.
(27) Empsall, H. D.; Hyde, E. M.; Markham, R.; McDonald, W. S.; Norton, M. C.; Shaw, B. L.; Weeks, B. *J. Chem. Soc., Chem. Commun.* **1977**, 589.
(28) Typical isotropic thermal B values for the axial ligand range from 5.9 for C(37) to 14 for C(40). See supplemental data for a full listing.
(29) Cocolios, P.; Guilard, R.; Bayeul, D.; Lecomte, C. *Inorg. Chem.* **1985**, *24*, 2058.
(30) Cullen, D. L.; Meyer, E. F.; Smith, K. M. *Inorg. Chem.* **1977**, *16*, 1179.
(31) Gouterman, M. In *The Porphyrins*; Dolphin, D., Ed.; Academic Press: New York, 1979; Vol. 3.

Table IV. Table of Selected Bond Angles of (OEP)Ir(C_8H_{13})

atom 1	atom 2	atom 3	angle (deg)	atom 1	atom 2	atom 3	angle (deg)
N_1	Ir	N_2	93.4 (3)	C_{38}	C_{37}	C_{44}	95.8 (8)
N_1	Ir	N_3	176.1 (3)	C_{37}	C_{38}	C_{39}	124.0 (1)
N_1	Ir	N_4	87.4 (3)	C_{37}	C_{38}	C_{42}	116.0 (1)
N_1	Ir	C_{37}	88.4 (3)	C_{39}	C_{38}	C_{42}	98.4 (9)
N_2	Ir	N_3	87.1 (3)	C_{38}	C_{39}	C_{40}	107.0 (1)
N_2	Ir	N_4	175.4 (2)	C_{39}	C_{40}	C_{41}	114.0 (1)
N_2	Ir	C_{37}	94.3 (3)	C_{40}	C_{41}	C_{42}	100.0 (1)
N_3	Ir	N_4	91.8 (3)	C_{38}	C_{42}	C_{41}	104.0 (1)
N_3	Ir	C_{37}	95.4 (3)	C_{38}	C_{42}	C_{43}	100.0 (1)
N_4	Ir	C_{37}	90.2 (3)	C_{41}	C_{42}	C_{43}	108.0 (1)
Ir	C_{37}	C_{38}	123.6 (8)	C_{42}	C_{43}	C_{44}	108.8 (9)
Ir	C_{37}	C_{44}	124.3 (6)	C_{37}	C_{44}	C_{43}	112.1 (8)

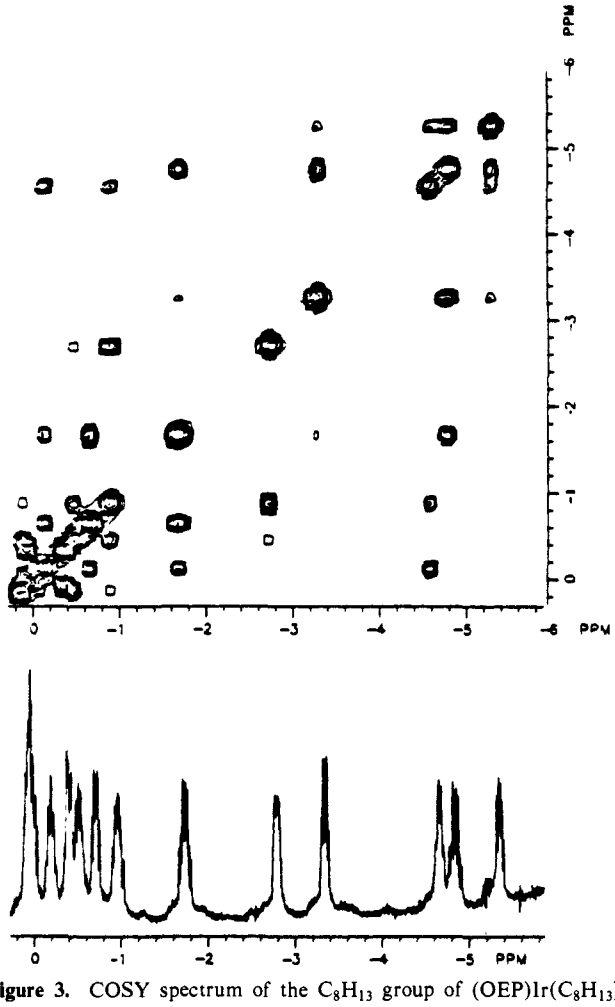

Figure 3. COSY spectrum of the C_8H_{13} group of (OEP)Ir(C_8H_{13}).

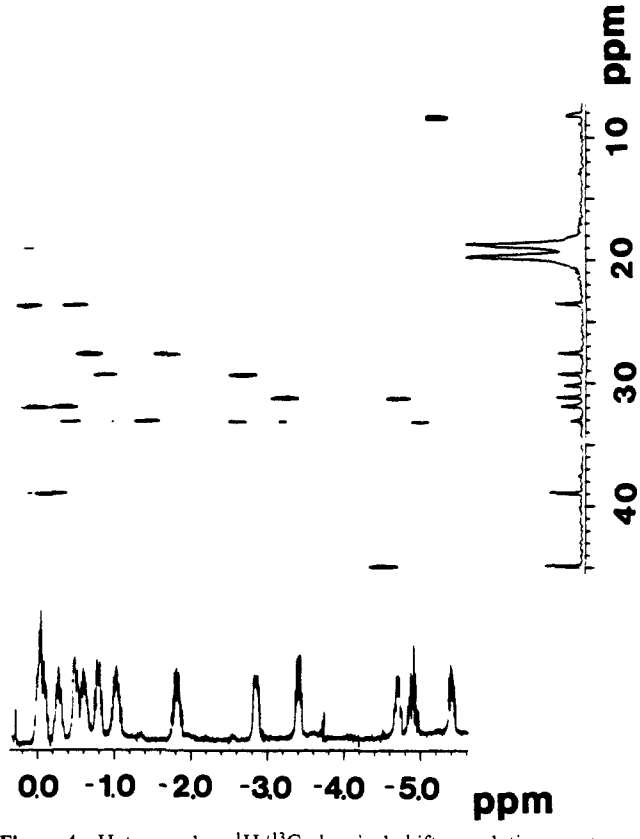

Figure 4. Heteronuclear $^1H/^{13}C$ chemical shift correlation spectrum, C_8H_{13} group of (OEP)Ir(C_8H_{13}).

structure, which shows all of the protons of this ligand to be close to the porphyrin.

An unambigious assignment of the resonances for the *cis*-bicyclo(3.3.0)oct-1-yl ligand is not possible from the ^1H NMR alone. However, by use of the COSY (Figure 3) and the Heteronuclear Proton–Carbon Chemical Shift Correlation techniques (Figure 4), both the ^1H NMR and the ^{13}C NMR spectra of this ligand could be completely assigned.

The $^1H/^{13}C$ correlation spectrum (Figure 4) gives three carbons correlated with only one proton. From the crystal structure, they are C(37), C(38), and C(42). These three carbons can be distinguished by consideration of proximity to the porphyrin plane. The closer the atoms are, the greater the upfield shift of the corresponding ^1H NMR signal. Hence, the resonance at -5.2 ppm is assigned to H(37) which implies that C(37) resonates at 8.18 ppm. By the same arguments the following assignment can be made: C(38) at 44.84 ppm and H(38) $\simeq$ -4.6 ppm; C(42) at 38.90 ppm and H(42) $\simeq$ -0.2 ppm. The assignment of C(38), H(38), and C(42), H(42) is in agreement with the COSY experiment (Figure 3), which indicates coupling between H(37) and H(38) and not between H(37) and H(42).

From the crystal structure (Figure 1b) strong coupling between H(37) and $H(44)_b$[32] is expected, and this is observed in the COSY spectrum. Since the ^1H signal at $\simeq$ -4.9 ppm is due to $H(44)_b$ from the $^1H/^{13}C$ correlation, C(44) resonates at 31.13 ppm, and the other proton on C(44), $H(44)_a$ resonates at $\simeq$ -3.4 ppm. By using the same arguments, each signal in the ^1H and ^{13}C spectrum was assigned, and the results are summarized in Table V. However, as shown in Figures 2 and 3, the complexity of the signal prevented determination of coupling constants. The ^1H NMR study is in complete agreement with the crystallographic data, and it can be concluded that the solution structure and solid-state structure are basically the same.

CO Addition Studies. The addition of CO to (OEP)Ir(C_8H_{13}) to give (OEP)Ir(C_8H_{13})(CO) was monitored by UV–vis and infrared spectroscopy in DCE and THF. Introduction of CO into an oxygen free solution of (OEP)Ir(C_8H_{13}) results in the appearance of a new peak at 2025 cm^{-1} in the infrared spectrum,

(32) The designation H(44b) corresponds to the proton on C(44) which is between the plane of porphyrin ligand and the C_8H_{13} ligand, while H(44a) would correspond to the proton above the C_8H_{13} ligand.

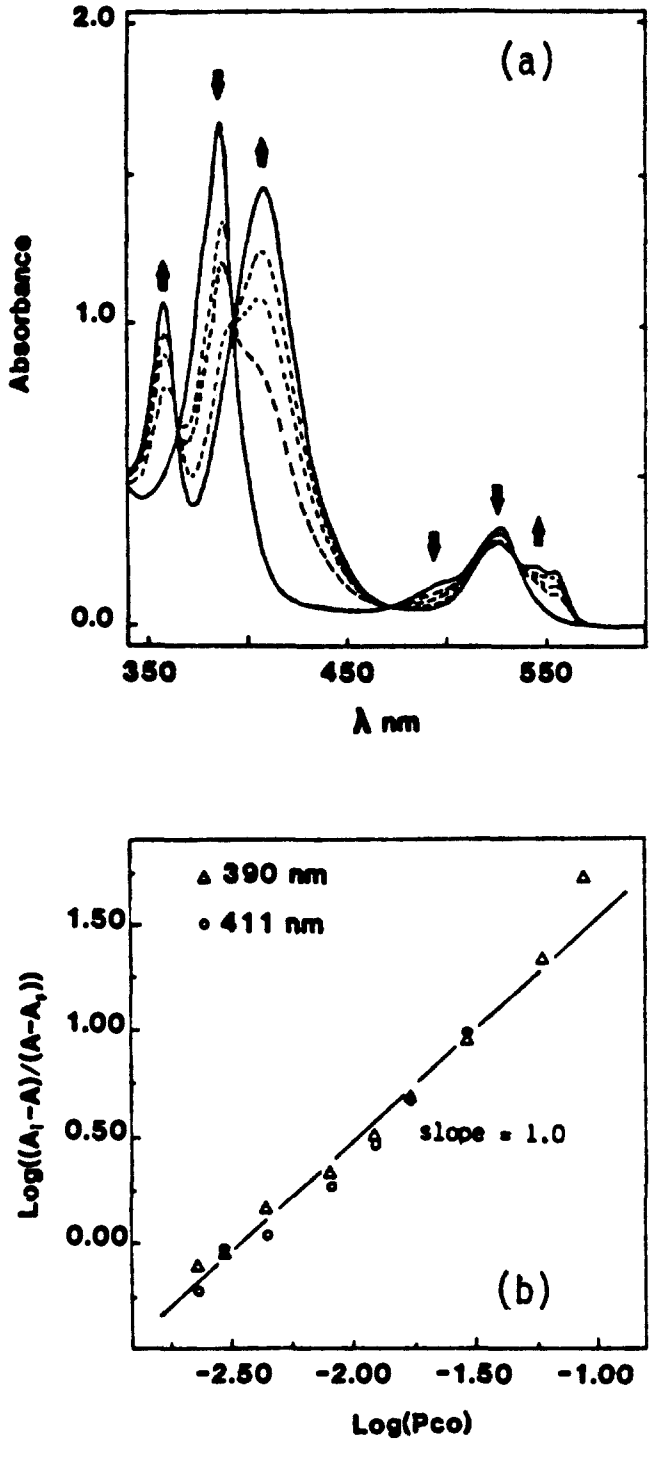

Figure 5. (a) UV-vis spectral changes and (b) plot of log $((A_i - A)/(A - A_f))$ vs. log (P_{CO}) for (OEP)Ir(C_8H_{13}) in DCE, 0.1 M TBA(ClO_4).

clearly due to the formation of an Ir–CO bond.

The CO addition reaction is reversible. If the solution of the CO adduct is degassed with argon for 3–4 min, the band at 2025 cm^{-1} disappears from the infrared spectrum. This band reappears again upon adding CO to solution, and the appearance/disappearance of the 2025-cm^{-1} band can be cycled many times. The frequency of the Ir–CO vibration is very similar to that reported for (OEP)Ir(CO)(CH_3),[3] where a band at 2022 cm^{-1} is observed. In addition, the infrared spectrum of (OEP)Ir(C_8H_{13}) does not indicate loss of the (C_8H_{13}) ligand upon complexation with CO.

Figure 5a shows changes in the UV-vis spectrum of (OEP)-Ir(C_8H_{13}) in DCE containing 0.1 M TBA(ClO_4) as a function of CO pressure above the solution. The initial product, under argon, has a Soret band at 390 nm and two visible bands at 495 and 528 nm. This is a typical electronic absorption spectrum for an octaethylmetalloporphyrin.[31] Upon addition of CO, the Soret band at 390 nm decreased in intensity while two new absorption bands appeared at 360 and 411 nm. At the same time, the band at 528 nm decreased in intensity while a broad absorption band appeared between 500 and 560 nm. This band was characterized by maxima at 527, 545, and 555 nm. Only one set of isobestic points is observed during the addition of CO to (OEP)Ir(C_8H_{13}). Analysis of the changes in the absorption spectrum as a function of CO pressure gave plots of the type shown in Figure 5b. The slope of the line in Figure 5b was 1.0, and from this data an equilibrium constant of K_1 = 340 ± 200 atm^{-1} was calculated for formation of the mono CO adduct (eq 1).

$$(OEP)Ir(C_8H_{13}) + CO \rightleftharpoons (OEP)Ir(C_8H_{13})(CO) \quad (1)$$

The above reaction was reversible and the original UV-vis spectrum could be recovered by bubbling argon through the solution.

Table V. Proton and Carbon Chemical Shift Assignment of the *cis*-Bicyclo(3.0.0)oct-1-yl Group of (OEP)IrC_8H_{13}[a]

position[b]		chemical shifts ^1H (ppm)[c]	^{13}C (ppm)
37	Hb	−5.2	8.18
38	Ha	−4.6	44.84
39	Ha	−0.9	29.26
	Hb	−2.8	
40	Ha	0.1	23.53
	Hb	−0.5	
41	Ha	0.1	31.87
	Hb	−0.4	
42	Ha	−0.2	38.90
43	Ha	−1.7	27.52
	Hb	−0.7	
44	Ha	−3.4	32.13
	Hb	−4.8	

[a] In Deuterated Benzene with the Observation Frequencies of 300.068 and 75.457 MHz. [b] See Figure 1 and ref 32 for numbering scheme. [c] Reported at 0.1 ppm due to the strong coupling.

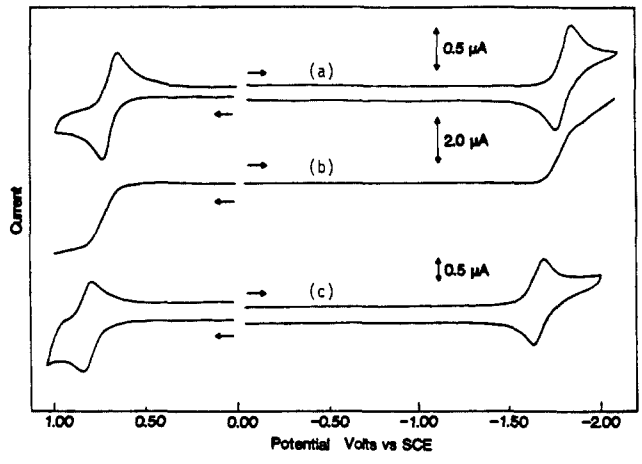

Figure 6. (a) Cyclic voltammogram and (b) rotating disk voltammogram of (OEP)Ir(C_8H_{13}) in THF, 0.1 M TBA(ClO_4). (c) Cyclic voltammogram of (OEP)Ir(C_8H_{13})(CO) in THF, 0.1 M TBA(ClO_4), P_{CO} = 1 atm.

Electrochemical Studies. Figure 6a shows a typical cyclic voltammogram of (OEP)Ir(C_8H_{13}) under an argon atmosphere in THF, 0.1 M TBAP. Two reversible one-electron processes[33] are observed at 0.68 V and −1.79 V vs. SCE. The voltammogram obtained by using a rotating disk electrode (Figure 6b) demonstrates that the electron transfers at 0.68 and −1.79 V are, respectively, an oxidation and a reduction. Similar electrochemical results are observed in DCE and THF, and Table VI summarizes the half-wave potentials observed in the two solvents. Due to the limited reduction potential window of DCE, the first reduction

(33) For both waves $|E_{pa} - E_{pc}|$ = 60 ± 5 mV, i_{pa}/i_{pc} = 1.00 ± 0.05 and $i_p/v^{1/2}$ = constant over the scan rate range of 0.05–5.0 V/s.

Table VI. Half-Wave Potentials (V vs. SCE) for the Reduction and Oxidation of (OEP)Ir(C_8H_{13}) and (OEP)Ir(C_8H_{13})(CO) in DCE and THF Containing 0.1 M TBA(ClO_4)

compound	solvent	oxidation	reduction
(OEP)Ir(C_8H_{13})[a]	DCE	0.67	
	THF	0.68	-1.79
(OEP)Ir(C_8H_{13})(CO)[b]	DCE	0.81	-1.70[c]
	THF	0.80	-1.65

[a] Under 1 atm Ar. [b] Under 1 atm CO. [c] Value given is E_{pc} at 0.10 V/s.

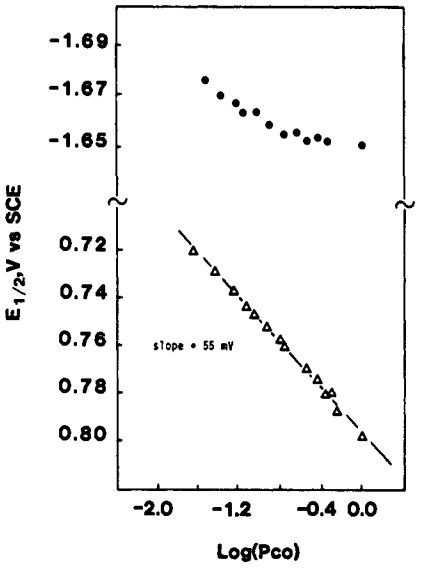

Figure 7. Plot of $E_{1/2}$ vs. log (P_{CO}) for the reduction and oxidation of (OEP)Ir(C_8H_{13}) in THF, 0.1 M TBA(ClO_4).

(observed at -1.79 V in THF) is poorly defined. Finally, Figure 6c shows the cyclic voltammogram of (OEP)Ir(C_8H_{13}) in THF under a CO atmosphere. Two reversible one-electron transfers are observed, and half-wave potentials for both processes are shifted positively compared to those of (OEP)Ir(C_8H_{13}).

An electrochemically monitored titration of (OEP)Ir(C_8H_{13}) with CO was performed, and the resulting plot of $E_{1/2}$ vs. log(P_{CO}) is shown in Figure 7. The observed value of $\Delta E_{1/2}/\Delta\log(P_{CO})$ is 55 mV for the oxidation, which implies the loss of CO upon oxidation of (OEP)Ir(C_8H_{13})(CO). The shift in $E_{1/2}$ for the reduction is due to the differences in equilibrium constants for bonding of CO to the neutral and reduced forms. From the differences between $E_{1/2}$ for the (OEP)Ir(C_8H_{13})/[(OEP)Ir(C_8H_{13})]$^-$ couple and $E_{1/2}$ for the [(OEP)Ir(C_8H_{13})(CO)]/[(OEP)Ir(C_8H_{13})(CO)]$^-$ couple and from K_1 (see reaction 1), the equilibrium constant $K_2 = 80 \pm 50 \times 10^3$ atm^{-1}, for reaction 2, can be calculated.

$$[(OEP)Ir(C_8H_{13})]^- + CO \rightleftarrows [(OEP)Ir(C_8H_{13})(CO)]^- \quad (2)$$

Controlled potential oxidation of (OEP)Ir(C_8H_{13}) was carried out in DCE, and the products were monitored by electronic absorption spectroscopy and ESR. Figure 8a demonstrates changes in the UV-vis spectra during the one-electron oxidation of (OEP)Ir(C_8H_{13}) in DCE. The Soret band of the oxidized species is blue-shifted and slightly increased in intensity. The visible bands are decreased in intensity and are slightly red-shifted. The original spectrum of (OEP)Ir(C_8H_{13}) is observed upon rereduction at potentials more negative than 0.50 V. Similar changes in the UV-vis spectra were observed in THF, and spectral data for each of the reduced, oxidized, and neutral species are summarized in Table VII. The ESR spectrum recorded after controlled potential oxidation of (OEP)Ir(C_8H_{13}) by one electron (1.0 ± 0.1) has a strong signal with a g value of 1.992. This asymmetrical signal has a total width of 31 G and a peak to peak separation of 6.5 G.

Figure 8b shows the UV-vis spectral changes upon oxidation of (OEP)Ir(C_8H_{13})(CO) under a CO atmosphere in DCE, 0.1 M TBA(ClO_4). The spectral changes are not reversible after the controlled potential oxidation of (OEP)Ir(C_8H_{13})(CO) under a CO atmosphere. No ESR signal is observed after this one-electron oxidation, and no current is passed when a potential of 0.00 V is applied after complete oxidation. In addition, the UV-vis spectrum does not change after applying a potential of 0.00 V, further indicating the irreversibility of this reaction.

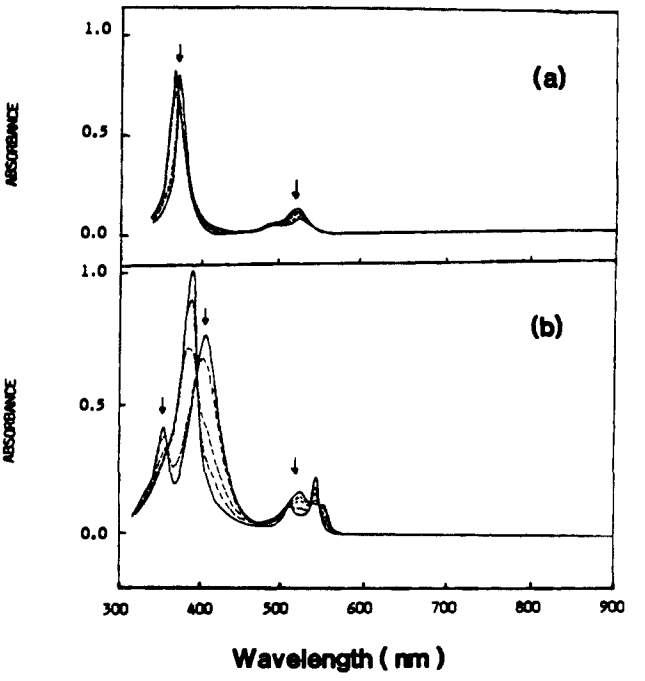

Figure 8. Changes in the electronic absorption spectra during controlled potential oxidation of (a) (OEP)Ir(C_8H_{13}) under argon and (b) (OEP)Ir(C_8H_{13})(CO) under CO in DCE, 0.1 M TBA(ClO_4).

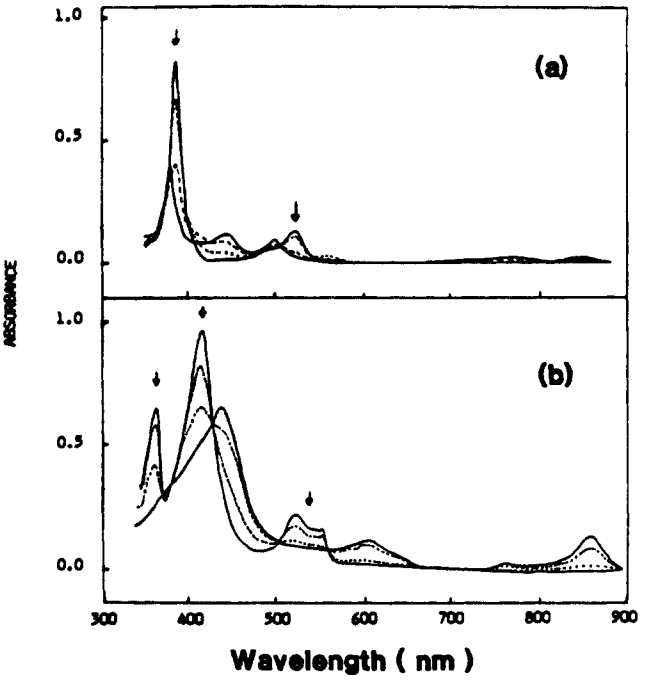

Figure 9. Changes in the electronic absorption spectra during controlled potential reduction of (a) (OEP)Ir(C_8H_{13}) under argon and (b) (OEP)Ir(C_8H_{13})(CO) under CO in THF, 0.1 M TBA(ClO_4).

The final spectrum of the first oxidation product is characterized by a Soret band at 394 nm and two visible bands at 512 and 545 nm and is identical with the UV-vis spectrum reported for (OEP)Ir(CO)(ClO_4).[2] This implies loss of the C_8H_{13} ligand upon oxidation of (OEP)Ir(C_8H_{13})(CO) under a CO atmosphere. Thus, (OEP)Ir(CO)(ClO_4) appears to be the final product on long time scale oxidation of (OEP)Ir(C_8H_{13})(CO). This species is stable

Table VII. Maximum Absorbance Wavelengths (λ_{max}) and Corresponding Molar Absorptivities (ϵ) for the Oxidized and Reduced Products of (OEP)Ir(C_8H_{13}) and (OEP)Ir(C_8H_{13})(CO) in DCE and THF, 0.1 M TBA(ClO_4)

compound	solvent	λ_{max}, nm ($\epsilon \times 10^{-3}$)			
(OEP)Ir(C_8H_{13})	DCE	390 (140)	495 (12)	528 (31)	
	THF	390 (137)	495 (9.4)	528 (22)	
[(OEP)Ir(C_8H_{13})]$^+$	DCE	387 (142)	496 (12.5)	530 (21)	540 (sh)
	THF	385 (139)	494 (9.5)	530 (15)	540 (sh)
[(OEP)Ir]$^{-1}$	THF	383 (73)	449 (31)	505 (22.8)	863 (5.1)
(OEP)Ir(C_8H_{13})(CO)[a]	DCE	360 (88)	411 (120)	527 (25)	555 (18)
	THF	360 (90)	411 (120)	524 (24)	554 (17)
(OEP)Ir(CO)(ClO_4)	DCE	394 (155)	512 (15)	545 (32.5)	
	THF	395 (154)	512 (15)	545 (32.2)	
[(OEP)Ir(C_8H_{13})(CO)]$^-$[a]	THF	438 (74)	608 (8.2)	864 (11.2)	

[a] Spectra obtained under 1 atm CO.

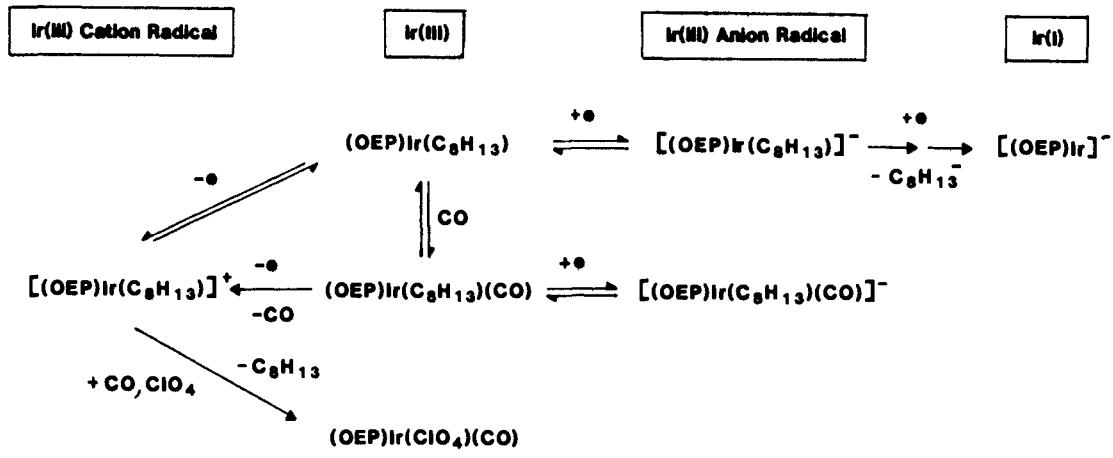

Figure 10. Electrode reactions of (OEP)Ir(C_8H_{13}) and (OEP)Ir(C_8H_{13})(CO).

as the Ir(III) complex and is not reducible until potentials more negative than −1.0 V vs. SCE are applied.

The reduction of (OEP)Ir(C_8H_{13}) proceeds by one or two electrons depending upon the time scale of the measurement. Only a one-electron transfer is observed by cyclic voltammetry and by rotating disk voltammetry (see Figure 6). In contrast, coulometry and controlled potential electrolysis indicate the addition of two electrons to (OEP)Ir(C_8H_{13}). The initial thin-layer, UV–vis changes during controlled potential reduction of (OEP)Ir(C_8H_{13}) in THF indicate formation of an anion radical. The Soret and visible bands decrease in intensity with the simultaneous appearance of new bands at 448, 770, and 863 nm. However, upon further reduction a new species is formed. The new species has a Soret band decreased in intensity and shifted to a shorter wavelength. The new band at 448 nm is slightly increased in intensity while the band at 863 nm has decreased in intensity. A new peak at 505 nm also appears. This is shown in Figure 9a.

Bulk electrolysis and coulometry were performed at −1.9 V and after the addition of 1.8 ± 0.1 electrons the same final UV–vis spectrum is obtained as in the thin-layer cell. The final reduction product does not have an ESR signal either at room temperature or at 120 K.

In contrast to (OEP)Ir(C_8H_{13}), controlled potential reduction of (OEP)Ir(C_8H_{13})(CO) indicates the reversible formation of an anion radical after the addition of one electron (1.1 ± 0.1). The spectra associated with this reduction are shown in Figure 9b. This reaction is reversible under a CO atmosphere, and the original spectrum of (OEP)Ir(C_8H_{13})(CO) could be regenerated by applying a controlled positive potential.

The overall sequence of steps in the oxidation and reduction of (OEP)Ir(C_8H_{13}) and (OEP)Ir(C_8H_{13})(CO) is shown in Figure 10. A reversibility of the electron transfer was observed on both thin-layer and bulk electrolysis time scales. This is in contrast to other known σ-bonded metalloporphyrins which lose the σ-bonded ligand on oxidation. This oxidation is best described as abstraction of an electron from the axial ligand. This description of the oxidation site is based on a number of observations. The typical UV–vis spectral changes associated with a porphyrin π cation radical are not observed.[34] In addition, the stability of the first oxidation product and the lack of any typical features of an *N*-alkyl(OEP) iridium complex[2] in the UV–vis spectra rules out the possibility of a migration reaction. The ESR signal with a *g* value of 1.992 and the lack of Ir hyperfine coupling does not suggest formation of an Ir^{IV} species.[35] Thus, this is the first example of an axial-ligand oxidation which does not result in cleavage of the metal–carbon bond.

(OEP)Ir(C_8H_{13})(CO) is also reversibly oxidized on the cyclic voltammetric time scale. The 55-mV slope in a plot of $E_{1/2}$ vs. log(P_{CO}) (Figure 8) for oxidation indicates formation of [(OEP)Ir(C_8H_{13})]$^+$ as the first oxidation product of the electrode reaction. However, on longer time scales formation of (OEP)-Ir(CO)(ClO_4) is spectrally observed. This means that the electrogenerated [(OEP)Ir(C_8H_{13})]$^+$ is not stable in the presence of CO but it does not imply direct reaction of CO with the Ir center.

The mechanism for formation of (OEP)Ir(CO)(ClO_4) is not known. However, the data suggest that CO reacts with the dissociation products of [(OEP)Ir(C_8H_{13})]$^+$ as shown in eq 3. The

$$[(OEP)Ir(C_8H_{13})]^+ \overset{-C_8H_{13}^{\bullet}}{\rightleftharpoons} [(OEP)Ir]^+ \xrightarrow{CO,\ ClO_4^-} (OEP)Ir(CO)(ClO_4) \quad (3)$$

formation of (OEP)Ir(CO)(ClO_4) would drive reaction 3 to the right. If this is the case, then the Ir–C bond in [(OEP)Ir(C_8H_{13})]$^+$ may not be as stable as the electrochemistry seems to imply. It may be that eq 3 is shifted to the left in the absence of CO and under these conditions [(OEP)Ir(C_8H_{13})]$^+$ is the major species spectrally observed after controlled potential oxidation.

The presence of bound CO also influences the stability of the reduction products. Spectroelectrochemical measurements indicate that the first reduction of (OEP)Ir(C_8H_{13}) and (OEP)Ir-(C_8H_{13})(CO) is at the porphyrin π ring system. This is suggested by the formation of absorption bands in the 600–900-nm range

(34) Kadish, K. M. *Prog. Inorg. Chem.* **1986**, *34*, 435–605.
(35) Harrison, B.; Logan, N.; Raynor, B. J. *J. Chem. Soc., Dalton Trans.* **1975**, 1385.

which are assigned to the anion radical.[34] However, at longer time scales, cleavage of the Ir-C bond occurs for $[(OEP)Ir(C_8H_{13})]^-$, and the final reduction product is $[(OEP)Ir]^-$ which is identified by its characteristic UV-vis spectrum. A chemical reaction does not occur after reduction of $[(OEP)Ir(C_8H_{13})(CO)]$, and the one-electron reduction yields an anion radical that is stable on long time scales.

The exact sequence of steps in the transformation of $[(OEP)Ir(C_8H_{13})]^-$ to $[(OEP)Ir]^-$ is not clear. The overall reaction is given by eq 4 and involves the transformation of an Ir(III)

$$(OEP)Ir(C_8H_{13}) + 2e \rightleftarrows [(OEP)Ir]^- + C_8H_{13}^- \quad (4)$$

porphyrin to an Ir(I) porphyrin. A similar overall two-electron reduction with loss of the σ-bonded ligand has been shown for (TPP)Co(R), but in this case a Co(II) intermediate is proposed.[36]

The intermediate in reaction 4 is an Ir(II) anion radical, and hence an intramolecular charge transfer must occur. For the case of $[(TPP)Co(R)]^-$, loss of the R^- group generates (TPP)Co(II) which is then immediately reduced.[36] A similar sequence of steps is possible for $[(OEP)Ir(C_8H_{13})]^-$, but in this case either the loss of ligand or the addition of the second electron would be accompanied by the intramolecular charge transfer. However, an alternate series of steps involving the addition of a second electron and subsequent loss of $C_8H_{13}^-$ from $[(OEP)Ir(C_8H_{13})]^{2-}$ cannot be ruled out if one assumes the intramolecular charge transfer to be the rate-determining step in the chemical reaction following the initial reversible one-electron addition.

Finally, it is important to note that the reduced six-coordinate $[(OEP)Ir(C_8H_{13})(CO)]^-$ is more stable than the reduced five-coordinate $[(OEP)Ir(C_8H_{13})]^-$. This may reflect the π acid nature of CO, the geometry of the iridium atom, or both. In any event, the binding of CO by the anion radical prevents further reduction to form a square planar Ir(I) complex.

(36) Fauvet-Perree, M.; Gaudemer, M.; Boucly, P.; Bevynck, J. *J. Organomet. Chem.* **1976**, *120*, 439.

Acknowledgment. The support of the National Science Foundation (Grant No. CHE-8515411) is gratefully acknowledged.

Registry No. $(OEP)Ir(C_8H_{13})$, 104575-68-0; $(OEP)Ir(C_8H_{13})(CO)$, 104575-69-1.

Supplementary Material Available: The cell packing diagram and full tables of bond angles, bond distances, atomic positions for all atoms including calculated hydrogen positions, hydrogen thermal parameters, and least-squares planes for the structural determination of $(OEP)Ir(C_8H_{13})$ and table of anisotropic thermal parameters (9 pages). Ordering information is given on any current masthead page.

Anion Complexation and Migration in (8-Silyl-1-naphthyl)boranes. Participation of Hypervalent Silicon

Howard Edan Katz

Contribution from AT&T Bell Laboratories, Murray Hill, New Jersey 07974.
Received July 1, 1986

Abstract: Compounds **1-3**, of general structure 8-RMe_2Si-1-Me_2B-naphthalene, were prepared, and their complexes with F^- were examined. The structure of **1**·F^- (R = Me) was determined by multinuclear NMR and X-ray crystallography, revealing an interaction between F^- and pentacoordinate Si. Syntheses of **2** (R = OEt) from dimethyl(8-iodo-1-naphthyl)silane and of **3** (R = F) from **2** proceeded via intramolecular anion migrations and hypervalent Si intermediates. Compound **2** is the only reported example of a silyl ether coordinated to a borane. The complex **3**·F^- was more stable than **1**·F^- because of increased participation of FMe_2Si in F^- bonding compared to Me_3Si. This work represents the first consideration of Si as a participant in bidentate anion complexation and the first exploration of bidentate Lewis acids in which the two active functional groups are different.

Multidentate effects in ionic complexation are of increasing interest and importance in enzyme modeling,[1] catalysis,[2] and ion transport.[3] While the complexation of cations may be accomplished with a variety of neutral *or* charged hosts, anion complexation has, until recently, been largely confined to the formation of inclusion compounds within positively charged cages.[4] In the past 2 years, bidentate coordination of anions by *neutral* organometallic compounds containing pairs of Lewis acidic functionalities has been achieved in the cases of mercury-,[5] tin-,[6] and boron-containing[7] hosts interacting with such guests as chloride, bromide, fluoride, hydride, and hydroxide. In all of these cases, the two Lewis acidic groups on a particular host were identical.

Among the many bidentate *cation* binders are compounds in which the two Lewis basic groups are not the same. For example, in the extremely simple case of aminoethers such as dimethyl(2-methoxyethyl)amine,[8] the nitrogen is clearly the more basic atom and is primarily responsible for coordination to cations and Lewis acids; however, the oxygen atom also contributes a bond

(1) Kellogg, R. M. *Top. Curr. Chem.* **1982**, *101*, 111-145. Katz, H. E. In *Stereochemistry and Energetics*; Verlag Chemie: Weinheim/Bergstr., in press.
(2) Weber, E.; Vögtle, F. *Top. Curr. Chem.* **1981**, *98*, 1-41. Wuest, J. P.; Zacharie, B. *J. Am. Chem. Soc.* **1985**, *10*, 6121-6123. Schmidtchen, F. P. *Chem. Ber.* **1984**, *117*, 1287-1298. Hine, J.; Linden, S.-M.; Kanagasabapathy, V. M. *J. Am. Chem. Soc.* **1985**, *107*, 1082-1083.
(3) Hardy, L. C.; Shriver, D. F. *J. Am. Chem. Soc.* **1985**, *107*, 3823-3828. Kaplan, M. L.; Rietman, E. A.; Cava, R. J., private communication.
(4) Dietrich, B.; Guilhem, J.; Lehn, J.-M.; Pascard, C.; Sonveaux, E. *Helv. Chim. Acta* **1984**, *67*, 91-104. Schmidtchen, F. P. *Chem. Ber.* **19818** *114*, 597-607.
(5) Wuest, J. P.; Zacharie, B. *Organometallics* **1985**, *4*, 410-411. Beauchamp, A. L.; Oliver, M. J.; Wuest, J. D.; Zacharie, B. *J. Am. Chem. Soc.* **1986**, *108*, 73-77.
(6) Newcomb, M.; Madonik, A. M.; Blanda, M. T.; Judice, J. K., private communication.
(7) Katz, H. E. *J. Org. Chem.* **1985**, *50*, 5027-5032.
(8) Clark, R. J. H.; McAlees, A. J. *Inorg. Chem.* **1972**, *11*, 342-348. Evilia, R. F.; Reilley, C. N. *J. Coord. Chem.* **1973**, *3*, 7-15. Langer, A. W., Jr.; Whitney, T. A. *U.S. Patent* 3734963; Reissue 28456, 1976.

0002-7863/86/1508-7640$01.50/0